

Article

On the Physical and Mechanical Responses of Egyptian Granodiorite after High-Temperature Treatments

Mohamed Elgharib Gomah ^{1,2}, Guichen Li ^{1,*}, Changlun Sun ³, Jiahui Xu ¹, Sen Yang ¹ and Jinghua Li ¹

¹ Key Laboratory of Deep Coal Resource Mining, School of Mines, China University of Mining and Technology, Ministry of Education of China, Xuzhou 221116, China; mohammedel-ghareeb.12@azhar.edu.eg (M.E.G.); tb20020033b31d@cumt.edu.cn (J.X.); ts20020064a31tm@cumt.edu.cn (S.Y.); ljhcumt@cumt.edu.cn (J.L.)

² Mining and Petroleum Engineering Department, Faculty of Engineering, Al-Azhar University, Cairo 11884, Egypt

³ Department of Future and Smart Construction Research, Korea Institute of Civil Engineering and Building Technology, Gyeonggi 10223, Korea; sunchanglun@kict.re.kr

* Correspondence: liguichen@cumt.edu.cn; Tel.: +86-158-0521-5566

Abstract: In the design and stability of thermal engineering applications, a thorough understanding of the evolution of damage in the rock following high-temperature treatments is crucial. Hence, this study investigates the influence of high temperatures on Egyptian granodiorite rock properties, given its widespread use as ornamental stones and aggregate material for roadways. Temperature effects up to 800 °C on its physical and mechanical responses were examined in conjunction with microstructure alterations. The results show that the density of granodiorite decreases after heat exposure due to a gain in volume and a loss in mass, with volume expansion being the most important component. In addition, the uniaxial compressive strength increases up to 400 °C before reducing linearly as the temperature increases, while the elastic modulus and P-wave velocity show a reducing trend with the temperature. This study suggests that granodiorite has a thermal damage threshold of 400 °C, beyond which its microstructure and physical and mechanical characteristics deteriorate, and granodiorite becomes less brittle and more ductile. Hence, at the mutation range (between 400 and 600 °C), the physical and mechanical responses shift from a stable to an unstable state. As a result, the microstructure of the granodiorite samples was destroyed at 800 °C, resulting in a significant drop in compressive strength and dilemmas in measuring the P-wave and elastic modulus. Accordingly, the findings of this study can be used to aid in the safe handling of this rock in high-temperature conditions.

Keywords: physical and mechanical responses; Egyptian granodiorite; thermal damage threshold; microstructure; thermal constructions



check for updates

Citation: Gomah, M.E.; Li, G.; Sun, C.; Xu, J.; Yang, S.; Li, J. On the Physical and Mechanical Responses of Egyptian Granodiorite after High-Temperature Treatments. *Sustainability* **2022**, *14*, 4632. <https://doi.org/10.3390/su14084632>

Academic Editor: Giovanna Pappalardo

Received: 25 February 2022

Accepted: 8 April 2022

Published: 13 April 2022

Publisher's Note: MDPI stays neutral with regard to jurisdictional claims in published maps and institutional affiliations.



Copyright: © 2022 by the authors. Licensee MDPI, Basel, Switzerland. This article is an open access article distributed under the terms and conditions of the Creative Commons Attribution (CC BY) license (<https://creativecommons.org/licenses/by/4.0/>).

1. Introduction

In recent decades, high-temperature rock mechanics have garnered considerable attention, particularly in geological engineering fields such as deep mining, geothermal energy extraction, nuclear engineering construction, coal mining, and hydrothermal systems [1–5]. The temperature in these thermal applications varies based on the type of environment. The temperature of a coal fire, for example, is usually between 700 and 900 °C [6,7]. Moreover, temperatures can extend to 1000 °C during coal gasification procedures [8]. Fire damage to rocks is also relevant to various sectors, including geomorphology, cultural heritage, civil works, and engineering geology. For example, in the case of a building fire, construction materials can be exposed to temperatures exceeding 700 °C [9]. Hence, the temperature has numerous effects on rocks' physical and mechanical properties [10], which leads to several inevitable problems to be solved in rock mechanics [11].

Recognizing the consequences of temperature on various rocks' physical and mechanical responses is of extraordinary significance for reducing the potential jeopardies generated by thermal damage and safety evaluation in rock engineering [12–16]. At high temperatures, all rocks are susceptible to deterioration. On the other hand, porous sedimentary stones tend to show less visible mechanical damage than dense, low-porosity rocks, specifically multi-mineral rocks like granites [17]. Furthermore, due to intrinsic mineralogical and textural varieties, the impact of the temperature on the alteration of the rock properties may differ among rocks of similar origins [18,19]. For example, high-porosity weathered granites may withstand higher temperatures than low-porosity fresh granites [20]. Therefore, the physical and mechanical behaviors of different kinds of stones after heat treatment have been investigated in some of the former literature, among them being granite [21–26], marble [27–29], sandstone [30,31], shale [32], salt rock [33], limestone [34,35], and mudstone [36–38]. Commonly, it has been observed that in all rocks that have been examined below their melting point, the physical and mechanical properties for them altered following heat treatment.

The physical responses [39] showed, for example, that the rates of mass loss, volume expansion, and density reduction increase as the temperature rises. Quartz's thermal expansion is very nonlinear, while the rest of the granodiorite-forming minerals, on the other hand, have linear temperature dependencies in their thermal expansion [40]. The mismatch of thermal expansion and the associated thermal stress within mineral grains subjected to high temperatures induce microcracks between and inside mineral particles [41], leading to rock structural damage. Hence, the ultrasonic wave velocity falls dramatically [42,43]. Some studies were primarily concerned with evaluating thermal damage from the microscopic approach. They detailed the internal mechanisms that modify rocks following a temperature rise that induces macroscopic property changes. For example, the authors of [44] investigated the P-wave velocity and microstructure modification of granite under open fire, concluding that microcrack creation is mostly responsible for reducing the P_v of granite as the temperature increases. In addition, the authors of [18] proposed that the chemical reactions in minerals during heating alter these physical properties of rock at high temperatures.

The uniaxial compressive strength (UCS) and elastic modulus (E) tests are most commonly used to evaluate mechanical rock properties in mining and civil engineering projects. However, the UCS and E tests have difficulties with direct measurements, including the necessity for accurate sample preparation and a large testing apparatus and the reality that these are destructive and time-consuming examinations [45,46]. On the other side, the mechanical responses of rocks may vary after thermal treatment [47–49]. Heat treatment can enhance or weaken rock strength within a specified temperature range [50–52]. Many researchers have examined the strength, deformation characteristics, and failure modes of rock that has been exposed to high temperatures [53–55]. For instance, depending on the rock type, structure, and mineral content, the peak strength of many rocks decreased by 40–60% with increasing temperatures (from 400 to 800 °C) [10,56]. According to [4], the stress–strain curves of Strathbogie granite showed plastic behavior at temperatures above 800 °C, and the brittle-plastic transformation has been observed under uniaxial compression between 600 and 800 °C. The authors of [24] performed uniaxial compression tests on granite to assess the impact of high temperatures on the crack damage and strength. They revealed that the crack damage threshold, strength, and static elastic modulus of granite increased at 300 °C before decreasing up to the max temperature of 800 °C.

Although the thermal damage of some rocks has been thoroughly explored, such as granite, marble, mudstone, and sandstone, systematic exploration of a new rock is crucial, and this research attempts to fill that gap. Hence, due to its rare experimental studies, the thermal damage impact on Egyptian granodiorite's physical and mechanical responses has been investigated. Granodiorite specimens were thermally treated at high temperatures up to 800 °C before being slowly cooled to ambient temperature. The experimental schemes started with estimating the initial physical properties of the

granodiorite specimens (e.g., density, size, mass measurement, and longitudinal wave). The next step was to subject each rock specimen to thermal processing by placing them in a high-temperature furnace with a temperature controller at the target temperatures. Afterward, the samples were gradually cooled to room temperature in the open air. Each rock specimen's physical parameters were then calculated once more. X-ray diffraction (XRD) and scanning electron microscopy (SEM) were used to illustrate the temperature-induced mineralogical changes and related microstructure degradation. Finally, the rock specimens were subjected to uniaxial compression examinations to examine the effect of thermal damage on the treated granodiorite's mechanical properties and failure patterns. These results will contribute as reference data for developing the knowledge of granodiorite rock thermal damage to predict and assess the stability and safety risks in thermal construction environments. As a result, a more realistic assessment of natural building stone thermal deterioration can be obtained.

2. Egyptian Granodiorite Rock

Granodiorites are coarse-grained igneous rocks with a grayish-white granularity and an intermediate composition between granite and diorite, with more plagioclase feldspar than orthoclase feldspar. Egyptian granite is divided into two types: young granite, which is pinkish to red in appearance and varies in kind from granitic to alkali granite, and old granite, which is dark gray and ranges from tonalite to granodiorite [57]. Due to settling in abundance in Egypt's eastern desert, the granodiorite stones were assembled from Egypt's Abo Marw region 130 km east of Aswan (Figure 1).

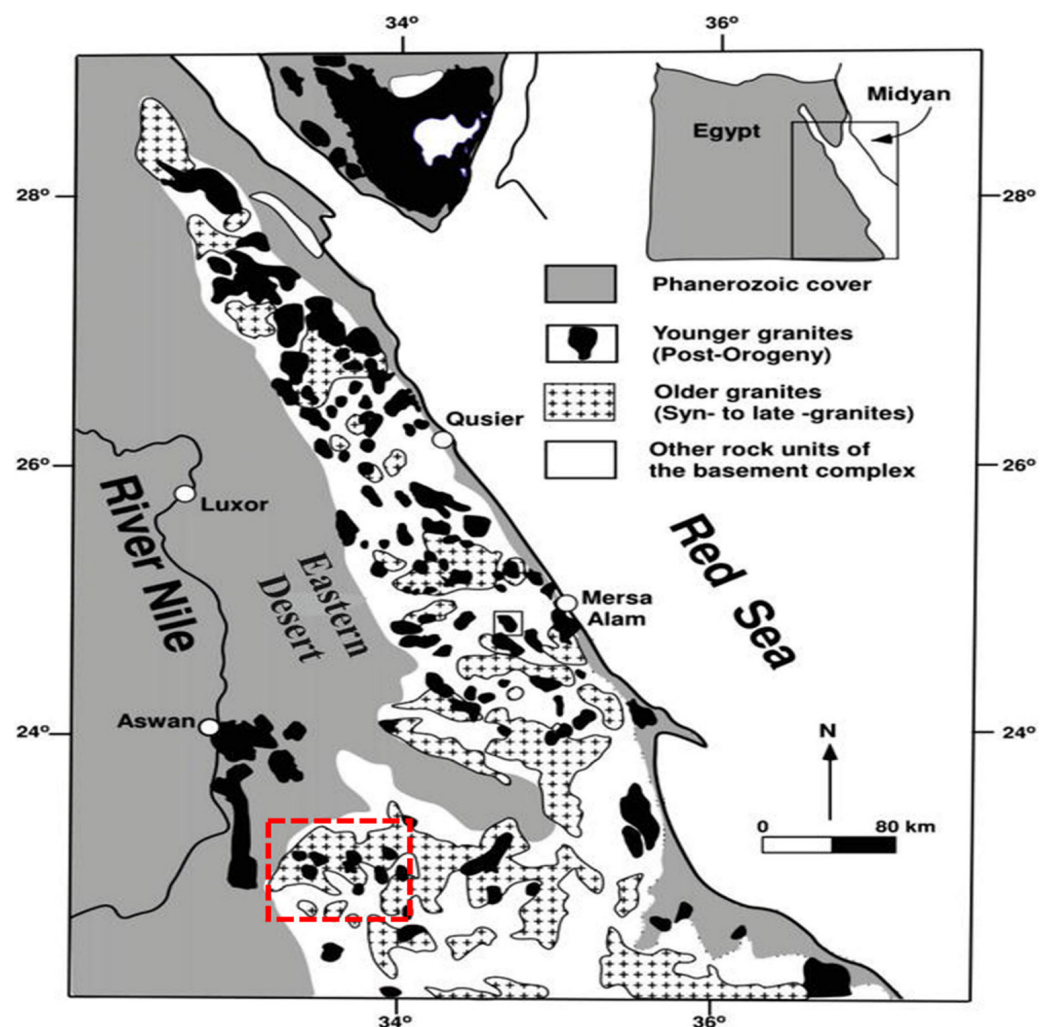


Figure 1. Map displaying the collection location of the granodiorite samples.

As a typical igneous rock widely used in modern constructions such as stairwells, hydro-engineering and bridges, road paving stones, architecture, and monuments, granodiorite's physical and mechanical properties when exposed to high temperatures were examined. Twenty-five cylindrical samples 55.5 mm in diameter and approximately 130 mm in length were drilled, following the standard the American Standard Test Method (ASTM) D7012–14 [58]. Granodiorite samples were prepared from cut blocks by the core-drilling machine. The granodiorite under study were fresh specimens distinguished by a gray color, with an average dry density of 2.69 g/cm^3 , and the main components included quartz, P-feldspar, K-feldspar, and biotite. Before testing, the samples were dried at $105 \text{ }^\circ\text{C}$ in the oven for at least 24 h to remove all moisture content.

3. Methods

3.1. Heat Treatment Process

Thermal treatments were performed on the granodiorite samples in a Nabertherm B410 electric furnace, with a maximum heating temperature of $1300 \text{ }^\circ\text{C}$ and a temperature control precision of $\pm 3 \text{ }^\circ\text{C}$ (Figure 2b). A modest heating rate of $5 \text{ }^\circ\text{C}/\text{min}$ was applied to minimize any potential thermal shock inside the specimens caused by the rapid temperature gradient [22,31,34]. Furthermore, the samples were maintained in the oven for 2 h after reaching the desired temperature to preserve the temperature uniformity within the specimens. The thermal effects on granodiorite were examined at five discrete spot temperatures: $200 \text{ }^\circ\text{C}$, $400 \text{ }^\circ\text{C}$, $500 \text{ }^\circ\text{C}$, $600 \text{ }^\circ\text{C}$, and $800 \text{ }^\circ\text{C}$. Finally, the specimens were then gently cooled to room temperature in "the open air". To determine the thermal loss rate of granodiorite throughout the cooling process following the thermal treatments at the target temperatures, the cooling rate and time required to reach room temperature for the air-cooled samples were monitored by a stopwatch and a contact thermometer (Figure 2c).



Figure 2. The principal used devices in this study: (a) P-wave velocity measurement tool, (b) Nabertherm electric furnace, (c) a contact thermometer, (d) uniaxial compression test machine, (e) the SEM apparatus, and (f) the XRD unit.

3.2. Mass, Volume, and Density Determination

Physical parameters such as the mass losses, volume expansion, and density reduction can quantify the extent of thermal damage induced in rock specimens after thermal treatment [50]. Hence, before and after heat treatment, the physical features of the studied granodiorite specimens were calculated. The samples were divided into 5 groups of “4 each”. Any test performed at least three times before the average value could be declared acceptable.

In this study, the mass loss rate η_m , volume growth rate η_V , and density decrease rate η_ρ were described as follows and as indicated in Equation (1):

$$\eta_m = (m_1 - m_2)/m_1 * 100\%, \eta_V = (V_2 - V_1)/V_1 * 100\%, \eta_\rho = (\rho_1 - \rho_2)/\rho_1 * 100\% \quad (1)$$

where m_1 , V_1 , and ρ_1 are the primary rock specimen’s mass, volume, and density, respectively, and m_2 , V_2 , and ρ_2 are the treated rock specimen’s mass, volume, and density, respectively.

3.3. UPV Measurements

The microstructural degradation of granodiorite caused by temperature was investigated using P-wave velocity calculations before and after thermal treatment. The elastic characteristics of rocks influence the dispersion of seismic waves by their mineralogy, texture, porosity, and cementation. As a result, knowing the size of the seismic waves in thermally treated rocks is crucial for their description [16]. Therefore, thermally induced microcrack degradation may be evaluated by equating the P-wave velocities before and after heat treatment. Hence, to measure the P-wave velocity along the specimen’s long axis, an ultrasonic pulse generation and acquisition system was employed in this study (Pundit PL-2 device (Figure 2a) with 2 54-kHz point-source transmitter-receivers). Vaseline was used to keep the transducers and specimen contacts together to ensure optimal energy transfer. Only samples with P-wave velocities that were comparable were selected. The measurements were performed five times for each specimen while following ASTM test designations (D2845), with the average P-wave velocity value chosen as the P-wave velocity value.

3.4. Mechanical Tests

Using a compression machine (CONTROLS) with a loading capacity of 200 T, a set of uniaxial compressive strength tests was executed on the thermally treated samples under uniaxial circumstances following ASTM D7012–14 specifications. The loading rate of the machine was reduced to a constant displacement rate of 0.05 mm per minute (Figure 2d). The stress–strain curve during axial compression was computed using the software ADVANTEST9, and the load was steadily grown at a constant pace until the sample failed in minutes. Two strain gauges and Linear Variable Differential Transducers (LVDTs) were used to measure the specimen’s axial and lateral deformation by strain meters during loading using a data collection system.

3.5. XRD and SEM Investigations

A scanning electron microscopy (SEM) examination evaluated the microcracks generated during the heating and cooling treatments. Thin sections of granodiorite specimens subjected to various treatments were employed to examine the growth of inter-granular and intra-granular cracks in the rock matrix. An FEI Quanta INSPECT-S device (Figure 2e) was employed in the SEM investigation to observe the granodiorite microstructure following thermal treatments, with magnifications ranging from 400 to 6000 \times . Using a Bruker D8 Advance X-ray diffractometer (Figure 2f), the mineral compositions of the powdered granodiorite samples were investigated from a starting position (2θ) of 5 $^\circ$ to an end position (2θ) of 89.9 $^\circ$ with a step size of 0.06 $^\circ$. The primary granodiorite content was determined by the diffraction data as follows: quartz (31%), plagioclase (39%), and K-feldspar (28%).

4. Results and Analysis

4.1. Thermal Loss of Granodiorite

In agreement with [59,60], the cooling rate for the specimens that cooled in the air was rapid at first due to the significant thermal loss, as seen in Figure 3, and the reduction had an exponential trend until the specimen approached room temperature. The cooling rates were 2.3, 3.1, 4, and 5.35 °C/min for 200, 400, 600, and 800 °C, respectively. The interesting point is that the air-cooled samples at 600 °C took a longer time to cool than those cooled at 800 °C, owing to surface microcracks that formed within and on the surface of the granodiorite specimens at 800 °C.

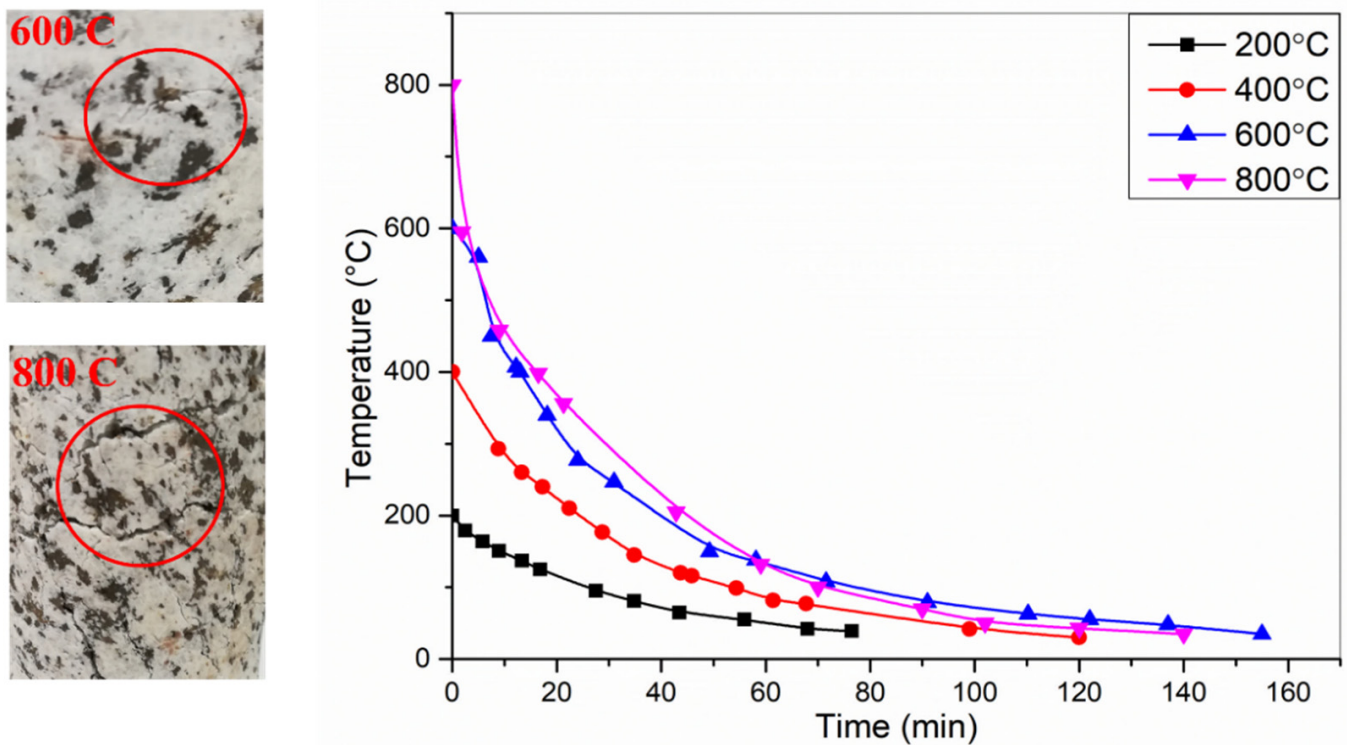


Figure 3. Cooling curves of the air-cooled samples at the target temperatures: 200, 400, 600, and 800 °C.

4.2. Temperature Effects on Mass, Volume, and Density

Figure 4 represents the variations in the mass loss ratio, volume growth rate, and density reduction ratio of the rock specimens exposed to thermal treatment. There are clear trends: the granodiorite's mass loss, volume expansion, and density decrease rates steadily increased as the temperatures rose. The mass loss of the granodiorite is predominantly due to the evaporation of various types of water [61]. Therefore, because of the low water content, the amount at which the granodiorite mass diminished with a temperature up to 400 °C was modest, as seen in Figure 4. For example, it extended to 0.09% and 0.14% at 200 and 400 °C, respectively (Table 1). In contrast, the volume expansion of the granodiorite had a meaningful value at this range of temperatures, reaching 1.6% at 400 °C.

Furthermore, there were similar values between the volume growth and density reduction rates, confirming its effectiveness in reducing the density. The mass loss, volume growth, and density reduction rates increased significantly over 400 °C, and the mass loss readings nearly doubled (0.31%), while the volume and density rates nearly tripled (5%) at 600 °C. As a result, this phase represents a mutation range for the deterioration of the parameters under investigation. At 800 °C, granodiorite's significant thermal degradation resulted in large reductions in the mass, volume, and density rates of 0.64%, 18.4%, and 16%, respectively.

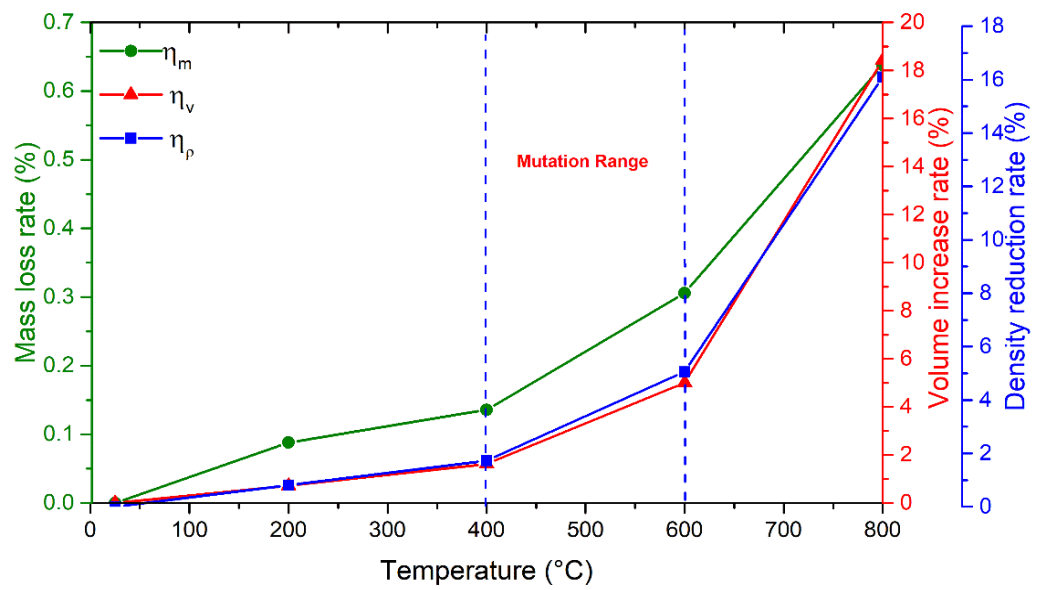


Figure 4. Relationships between average values of the mass loss rate (η_m), volume growth rate (η_v), and density decrease rate (η_p) for the target temperatures.

Table 1. Measured values of granodiorite physical parameters at various temperatures, where η_m is the mass loss rate, η_v is the volume growth rate, η_p is the density decrease rate, V_p is the P-wave velocity, $V_p\%$ is the P-wave loss ratio, and D. F (V_p) is the damage factor for the P-wave velocity.

Temperature (°C)	η_m (%)	η_v (%)	η_p (%)	V_p (m/s)	V_p (%)	D. F (V_p) (%)
25	0	0	0	5620	0	0
				5645		
				5518		
				5634		
				5593		
200	0.10	0.69	0.75	4415	22.55	0.40
	0.10	1.23	1.30	4420	20.73	0.37
	0.06	0.37	0.46	4461	19.33	0.35
	0.09	0.61	0.69	4519	20.74	0.37
400	0.13	1.58	1.68	3404	38.59	0.62
	0.13	1.57	1.67	3480	38.51	0.62
	0.15	1.61	1.72	3231	42.74	0.67
	0.14	1.73	1.85	3243	41.35	0.66
600	0.25	4.64	4.79	840	85.24	0.98
	0.31	6.12	6.01	888	84.60	0.98
	0.38	4.76	4.84	783	86.44	0.98
	0.28	4.51	4.58	795	86.26	0.98
800	0.50	18.49	16.03	1.00
	0.77	17.81	15.77	1.00
	0.64	18.97	16.49	1.00

4.3. Ultrasonic Velocity

Figure 5 demonstrates that as the temperature rose, the P-wave velocity of the granodiorite exhibited a thoroughly negative trend [62], diminishing when the temperature increased. There are three phases to the longitudinal velocity vs. temperature curve: up to 400 °C, 400–600 °C, and above 600 °C (Figure 5a,b). The V_p decreased markedly between the ambient temperature and 400 °C. For example, V_p diminished from 5606 m/s at room temperature to 4454 (with a 21% loss ratio) and 3340 (40% loss ratio (Table 1)) at 200 and 400 °C, respectively. The number of microcracks generated increased as the thermal treatment temperatures went up. As a response, the P-wave velocity dropped, since sonic waves travel slower in the air than in rock. Hence, 400 °C was considered the threshold point of the P-wave velocity measurements. It is noticeable that the P-wave reduced significantly after 400 °C, mainly between 400 to 600 °C, where the reduction rate was the sharpest (Figure 5b). Therefore, the average P-wave measurements at 600 °C were 826 m/s, with an 86% decrease ratio. Furthermore, the severity of the thermal cracks made measuring the longitudinal wave velocities impossible beyond 600 °C (predicted 0 m/s at 800 °C).

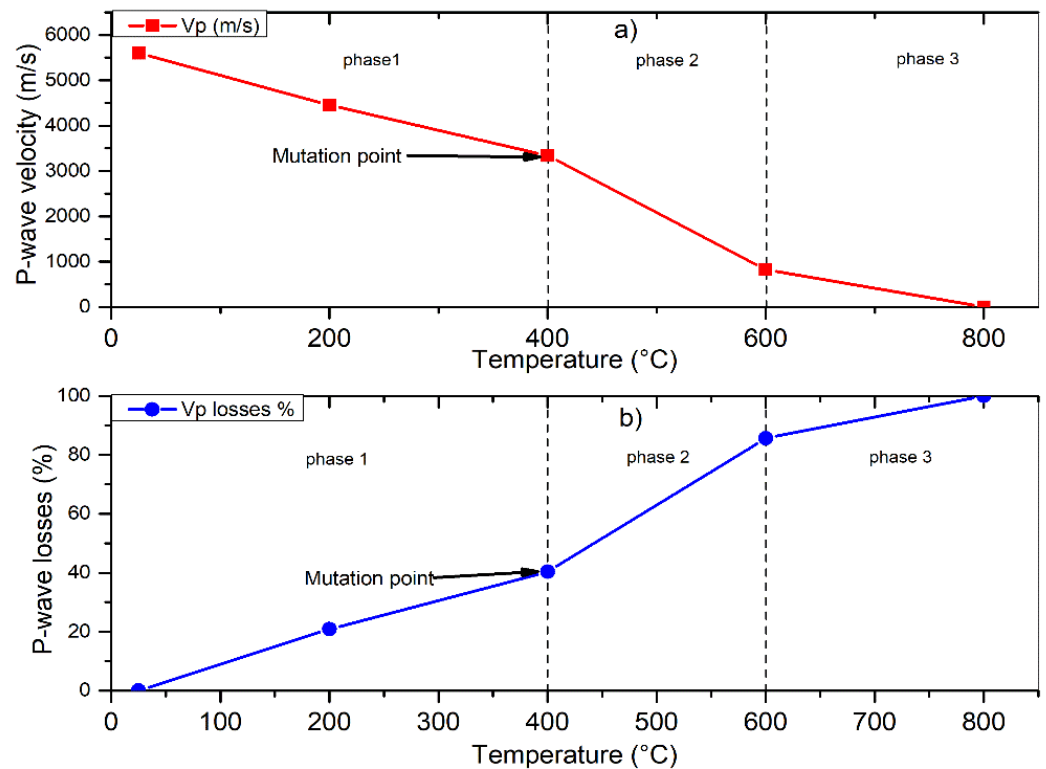


Figure 5. Relation between temperatures: (a) P-wave velocity and (b) P-wave loss ratio.

4.4. Temperature Effects on Mechanical Properties

4.4.1. Uniaxial Compressive Strength (UCS)

The compressive strength of granodiorite was investigated from the ambient temperature to 800 °C (Figure 6). Heat treatment can enhance rock strength by causing plastic expansions of minerals and strengthening friction among the mineral particles within a specified temperature range [50,51]. As a result, up to 400 °C, the granodiorite demonstrated a slowly rising trend, with the temperature and peak stress increasing by 5.74 MPa from 62.7 MPa to 68.44 MPa at 200 °C and 7.8 MPa at 400 °C, respectively. The principal motivation is that the granodiorite's granules slide less, owing to water evaporation and thus the presence of dry air within it. Furthermore, due to the thermal expansion of the interior mineral components, the initial cracks were also filled. Accordingly, microcracks were less frequent, and densification was better [63]. Therefore, the temperatures significantly impacted the granodiorite peak strength, which increased as the temperature was

less than 400 °C. When the temperature exceeded 400 °C, the related impact of thermal stress and applied uniaxial compression caused a significant creation of new microcracks to form, leading the granodiorite specimen to disintegrate. Consequently, the granodiorite compressive strength dropped dramatically from 70.2 MPa to 20.12 MPa at temperatures between 400 °C and 600 °C, a loss of 71%.

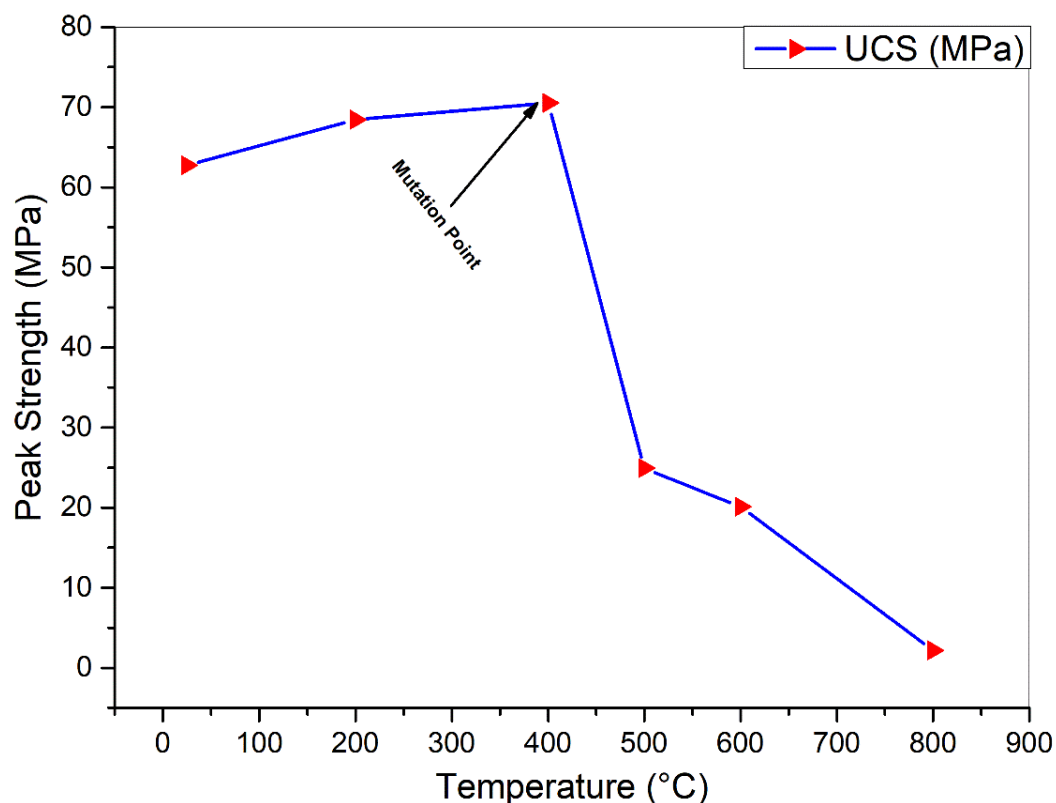


Figure 6. The variation of granodiorite's uniaxial compressive strength (UCS) following thermal treatment.

Moreover, between 400 °C and 600 °C, the quartz alpha-beta transition occurred at about 573 °C, resulting in a further steep drop. This suggests that 400 °C is the critical temperature for granodiorite microstructural and UCS modification. The peak stress distinctly reduced to 2.5 MPa at 800 °C (Table 2) due to various minerals starting to disintegrate and forming new microcracks, resulting in extensive macro-structural damage in the granodiorite.

4.4.2. Elastic Modulus (E)

Based on the empirical data for the granodiorite samples after thermal treatment, as illustrated in Figure 7, the elastic modulus reached its peak of 48.2 GPa at ambient temperature. From 25 °C to 400 °C, the elastic modulus of the granodiorite dropped by 41%. Thus, the governing causes in this stage were crystal and structural water evaporation, crack formation, and compressive deformation. Between 400 and 600 °C, the elastic modulus declined by 88% from 28.5 GPa to 5.6 GPa. These higher temperature ranges impaired the cohesiveness of the mineral grains, leading to thermal softening and causing microstructural degradation across the rock, ending in a notable decline in the elastic modulus. The E measurements were impossible after 600 °C because of severe degradation in the granodiorite specimens, as evidenced by the lower values of its UCS at this temperature range (Table 2).

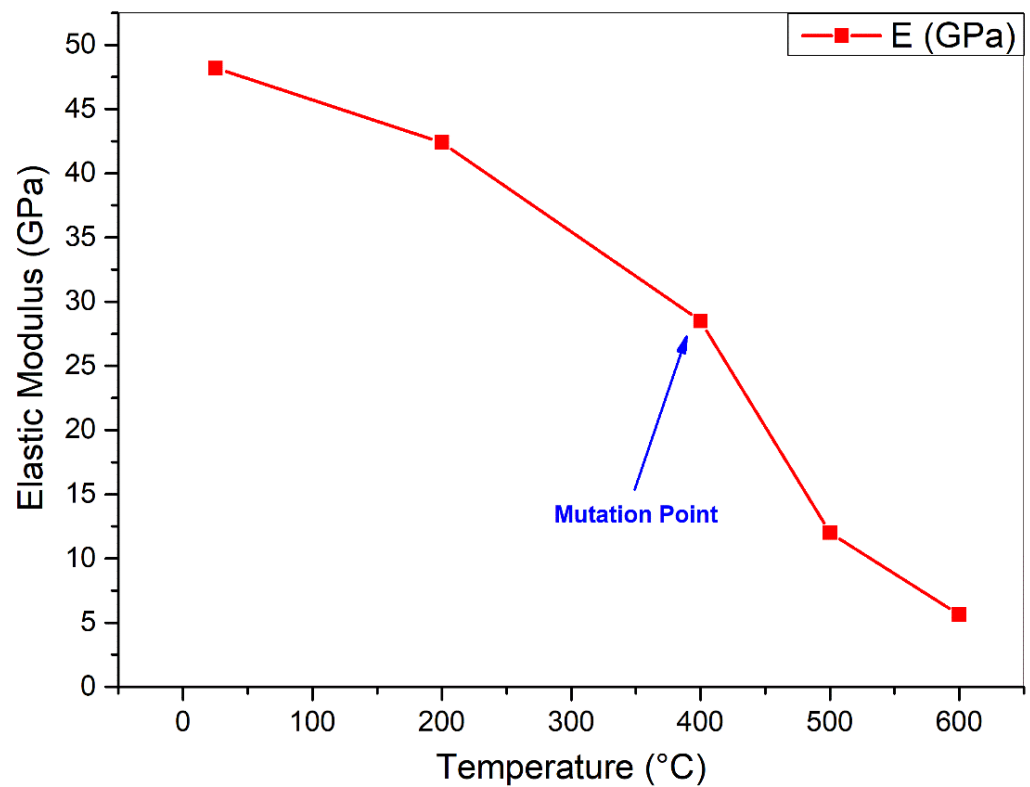


Figure 7. The variation of granodiorite's elastic modulus (E) with the temperature.

Table 2. Calculated values of granodiorite's mechanical parameters at different temperatures.

Temperature (°C)	Peak Strength (MPa)	Av. (USC) (MPa)	Elastic Modulus (GPa)	Av. (E) (GPa)	Thermal Damage (E) (%)
25	66.9	62.7	50.7	48.2	0.00
	65.9		47.8		
	59.2		48.0		
	59.0		46.2		
200	66.8	68.4	42.3	42.4	0.12
	63.5		39.7		
	75.0		45.2		
400	71.6	72.2	25.5	28.5	0.41
	74.2		24.7		
	70.8		35.3		
500	21.48	24.9	13.70	12	0.75
	28.39		10.30		
600	18.4	20.1	4.10	5.63	0.88
	23.0		9.60		
	18.9		3.20		
800	2.5	2.5	1.00
	Failed		...		
	2.6		...		

4.4.3. Stress–Strain Curves

Figure 8 shows the axial stress–strain curves by the LVDTs for the granodiorite specimens following various thermal treatments. As verified, the temperatures had a significant effect on the strength and deformation attributes of the granodiorite. Hence, the granodiorite’s axial stress–strain curves revealed a nonlinear deformation at first, which was induced by the closing of pre-existing microcracks. Furthermore, the temperature treatments impacted this phase (i.e., when the temperature rose, the stage of the first nonlinear deformation became more apparent). The increased number of thermal cracks caused by higher temperatures was most likely responsible. The linear regions dominated the stress–strain curves following the microcrack closure stage during the elastic deformation phase. With increasing axial stress, the stress–strain curves of the granodiorite began to deviate from the linear characteristics, indicating specimen yielding. The specimens then attained peak strength and started the post-peak deformation period.

As demonstrated in Figure 8, as the temperature rose, the brittleness diminished, and the ductility increased. The axial stress–axial strain curves of the granodiorite at lower temperatures (25–400 °C) exhibit apparent brittleness following the peak strength. The stress–strain curves were comparable under compression loading until the elastic deformation. In this zone, the stress–strain response was linear, with a rise in axial stiffness. In contrast, at higher temperatures (500 and 600 °C), the post-peak response of the granodiorite was more ductile, which was connected to the concentration of thermal cracks inside the specimens. Hence, after the elastic stage, visible plastic deformation occurred, during which the plastic characteristics of the granodiorite increased and the brittle properties diminished with the increasing temperature. Consequently, it has been revealed that as the temperature went up, the failure behavior shifted from a brittle to ductile shear zone. Additionally, on the granodiorite stress–strain curves, there are several stress mutations points due to the interconnection and nucleation of microcracks during the loading process, which is commonly described as an indicator for local failures [64].

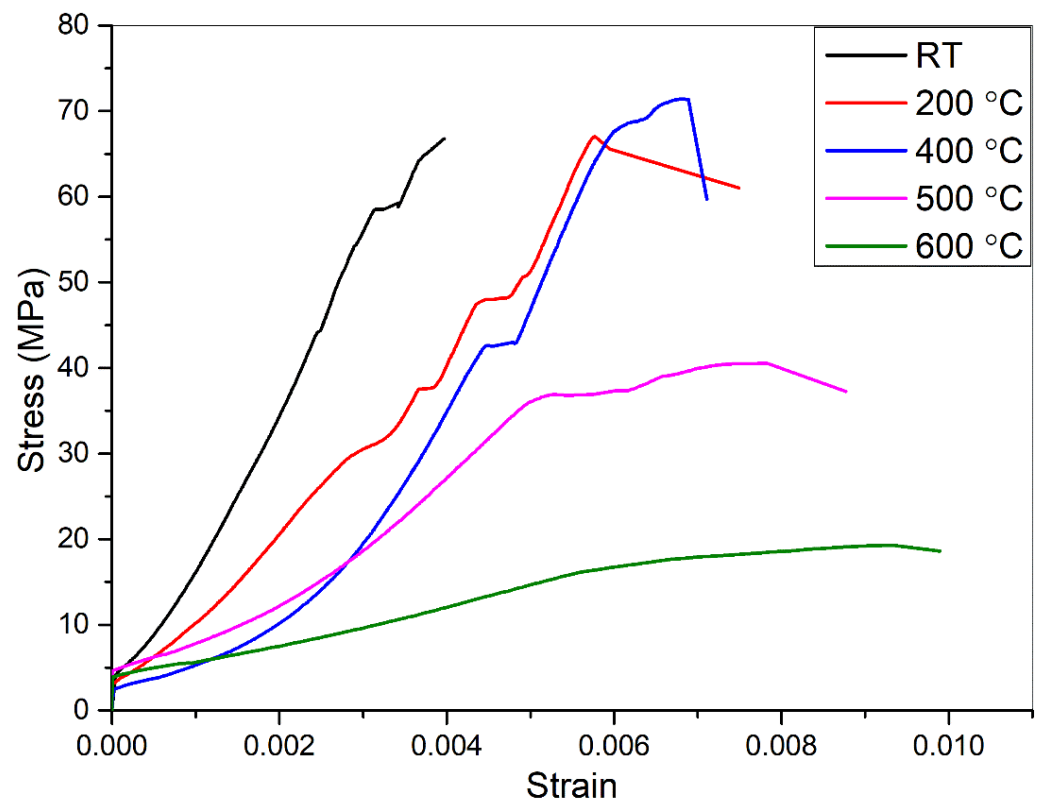


Figure 8. Stress–strain curves for granodiorite following different thermal treatments.

4.4.4. Failure Modes

Visual assessment for the post-failure samples revealed valuable information regarding the behavior of the tested rock samples at various temperatures. Various failure mechanisms involve inherent mechanical features such as the quantity of energy liberated throughout the failure and microstructural modifications during deformation. As a result, knowing the rock failure mechanisms at various temperatures is critical in anticipating failure mechanisms at different temperatures [4]. The failure modes after the compression stress of the thermally heated granodiorite specimens at various temperatures were compared and investigated. The failure mechanisms of the preheated granodiorite samples at 200, 400, 600, and 800 °C are shown in Figure 9a–d, respectively. It appears that as the temperature increased, the axial splitting failure mode at 200, 400 °C (Figure 9a,b) transformed to a shear failure mode at 600 °C (Figure 9c) due to the concentration of thermal cracks in the samples, in agreement with the stress–strain curves (Figure 8). The failure mode of the granodiorite was very complex at 800 °C, and many samples failed before the UCS tests, as shown in Figure 9d, due to the sharp degradation in the specimens.



Figure 9. Failure modes of granodiorite samples at various thermal treatments: (a) 200 °C, (b) 400 °C, (c) 600 °C, and (d) 800 °C.

4.5. Microstructural Evaluation

After being exposed to different temperatures (200, 400, 600, and 800 °C), SEM investigations were performed on the granodiorite specimens to assess any microstructural alterations, as shown in Figure 10. At 200 °C, the granodiorite specimens maintained their integrity (Figure 10a), with the mineral grains tightly linked and hairline cracks visible. When the temperature approached 400 °C, the granodiorite structure was subjected to significant thermal stresses due to different thermal expansions and water escaping. Therefore, the granodiorite's microstructure deteriorated as the temperature increased, and pores and intergranular cracks appeared, along with the emergence of intragranular cracks (Figure 10b). Due to the significant destruction of the microstructure, the cracks expanded considerably in width and length at 600 °C, and their frequency increased dramatically, as illustrated in Figure 10c. For the 800 °C specimens, the sample integrity crashed, and many thermal microcracks joined and coalesced, leading to substantially larger macroscopic crack densities and lengths compared with the specimens at 600 °C (Figure 10d).

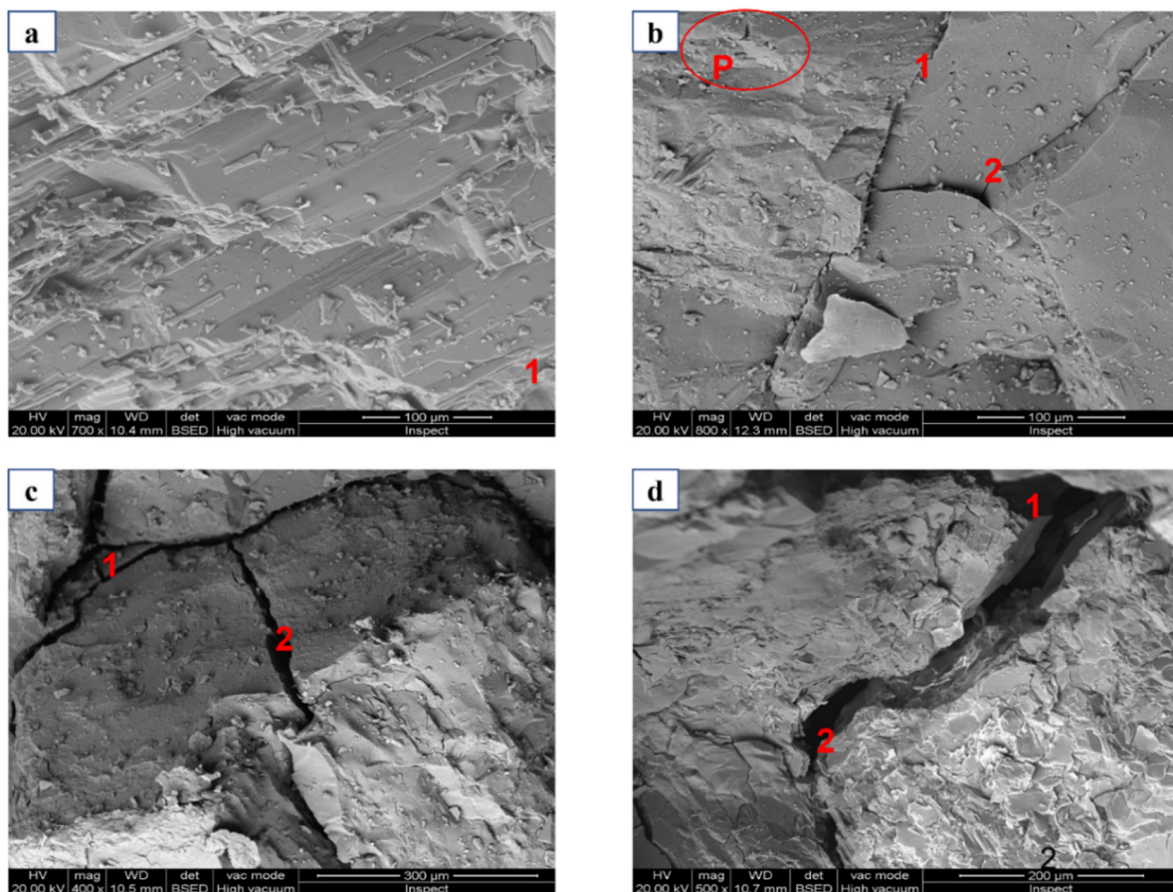


Figure 10. SEM images of granodiorite samples at various thermal treatments: (a) 200 °C, (b) 400 °C, (c) 600 °C, and (d) 800 °C. The abbreviations used are as follows: 1 = intergranular microcracks, 2 = intragranular microcracks, and P = pores.

5. Discussion

In this article, the thermal damage of several physical and mechanical characteristics following thermal treatments of Egyptian granodiorite were investigated, assessed, and compared with some previously published research, and all parameters that were measured mirrored this impact. Furthermore, regarding the responses at temperatures above 400 °C, the thermochemical processes dramatically promoted fracture damage creation and propagation, suggesting a potential trend.

5.1. Physical Responses as a Function of Temperature

Physical characteristics like the density, for example, are a reliable indicator for measuring the degree of damage produced in rock samples following thermal treatment [50]. When rock is heated, it undergoes several modifications; the size, shape, and mass of the sample change, leading to a shift in the volume and bulk density of the specimen. Hence, the density can be evaluated by comparing the volume and mass of the granodiorite samples before and after thermal treatment. The weight loss of granodiorite is mostly motivated by the evaporation of various kinds of water during heat treatment. Because granodiorite has a low water level in this temperature range, changes in the rate of mass decline were negligible at temperatures up to 400 °C. Hence, the losses in weight were restricted to the vaporization of interlayer water and bound water [61]. Beyond 400 °C, the mass loss rate rose considerably, suggesting that the granodiorite specimens' interior minerals suffered severe physical and chemical changes (Figure 4). In this mutation range, the crystalline water quantities decreased due to mineral dehydration, and the structural water contents declined due to dehydroxylation. Furthermore, decomposition of the opaque minerals and quartz, as well as feldspar phase shifts and recrystallization of the minerals distinguished these zones. At 600–800 °C, the mass loss rates were the greatest (Table 1), reflecting those chemical reactions which were the most pronounced [19].

On the other hand, the quartz transition is a common attribute in the volume expansion curve. It affects the granodiorite's thermal expansion slope, since it is a quartz–feldspar rock rich in silica. Consequently, between 25 and 400 °C, there was no substantial volumetric growth in the granodiorite samples, and the volume expansion was lineal and primarily attributable to the mineral extension [65]. Nevertheless, with the continuous development of minerals for temperatures above 400 °C, the volume expansion ratio of the rock samples accelerated dramatically, and the minerals' boundaries cracked. Therefore, there was a nonlinear volumetric increase (Figure 4). As a result, the volume expansion rate rose sharply at 600 °C due to the quartz suffering a transition of an α -quartz to β -quartz phase at around 570 °C, and transgranular cracks evolved quickly at this stage and extended in volume; hence, the volumes expanded considerably. Consequently, between 400 and 600 °C, the physical parameters shifted from a stable to an unstable state in this mutation range. Because of the severe thermal damage to the granodiorite, the peak that reflected the volumetric expansion occurred between 600 and 800 °C. Correspondingly, the combined impact of the mass and volume shifts influenced the density levels. Accordingly, the density levels were altered by the combined impact of the mass and volume variations. However, the observed density drop rate corresponded to the increase in the volume growth rates, implying that the volume expansion had a greater effect on the density than the mass losses, as shown in Figure 4. Thus, up to 600 °C, the volume growth rate and density decline ratio had approximately similar values. When over 600 °C, the density reduction ratio was influenced by high rates for the mass losses and volume rise ratios, resulting in a significant increase in the density drop rate.

V_p was affected by the type of rock, grain size and shape, density, porosity, water content, clay concentration, and temperature, among other factors [66]. Hence, the longitudinal wave velocity dropped as the temperature rose, implying that the sonic wave energy values were progressively reflected and absorbed into the granodiorite specimens, as seen in Table 1. Up to 400 °C, the water loss and volume expansion were accelerated by the thermal treatment, which grew the porosity of the granodiorite. Hence, the longitudinal wave's energy levels were consumed, resulting in a gradual reduction in the wave velocity. Between 400 and 600 °C, more water escaped, boundary cracks developed, and the minerals underwent significant chemical and physical changes. Furthermore, the crystals suffered transgranular cracks, severely forcing the wave velocity to fall. The longitudinal wave's loss ratio was extremely high in this phase, and V_p was very low, suggesting that the cracks absorbed the bulk of the longitudinal wave's energy (Figure 5). Thus, the mutation point of longitudinal wave absorption began after the 400 °C limits. The impacts of high temperatures were more pronounced at 800 °C, and the transgranular cracks widened quickly.

In addition, the inner structures of the granodiorite specimens were destroyed, leading to the absorption of the whole longitudinal wave and barring them from penetrating the rock specimens.

Microscopically, thermal fractures in crystalline rocks are usually caused by two main mechanisms: (1) a mismatch in the thermal expansion coefficients between different mineral granules (causing intergranular cracks) and (2) anisotropy of thermal expansion within single minerals (causing intragranular cracks) [67,68]. The heat treatment alters the microstructures of the rocks, allowing microcracks to emerge and propagate. As seen in Figure 10, the quantity and breadth of microcracks inside the granodiorite specimens increased dramatically as the temperature rose. Accordingly, the matrix's compaction and integrity were significantly thermally damaged. Due to the various minerals with different thermal properties in granodiorite, thermal expansion mismatches form between particles, causing unequal thermal stresses, which exacerbate and expand the microcracks. The more substantial thermal expansion occurs as the temperature rises. As a result, intragranular and transgranular microcracks emerge one after the other, and the initial microcracks tend to extend along the weak areas to become larger [69]. Thus, granodiorite underwent relatively minimal chemical and structural changes at lower temperatures, which created small expansion of the pre-existing microcracks and new cracks (Figure 10a). The intergranular cracks grew, and the transgranular cracks formed when the temperature rose to 400 °C (Figure 10b) due to bound water loss, dihydroxylation in the absence of constitutional water, and solid mineral growth. Hence, thermally generated cracks resulted from significant thermal stresses by differential elongation of the minerals along the crystal axes as the temperature rose, which formed when the thermal stress surpassed the maximum strength among or inside the minerals, resulting in damage to the microstructures. For example, under atmospheric pressure, the transition of α -quartz to β -quartz at 573 °C produced a linear expansion of 0.45% of the quartz [40]. Therefore, the intragranular cracks extended because of the intense volumetric growth of grains at 600 and 800 °C, and a microcrack network was generated in the specimen as the intergranular and transgranular microcracks coalesced (Figure 10c,d).

5.2. Mechanical Properties as a Function of Temperature

High temperatures altered the physico-chemical characteristics of the water and minerals in the rocks, causing changes in the density, content, structural properties and start and spread of microcracks as well as a change in the mechanical response [70]. Hence, rock strength, or failure stress in uniaxial compression tests, is a fundamental indicator of thermal rock mechanical deterioration. The granodiorite strength was enhanced between 25 and 400 °C because of heat treatment (Figure 6), generating an axial splitting failure mode (Figure 9). This was mainly due to plastic expansions of the minerals and strengthening friction among the mineral particles within a specified temperature range [50]. Evaporation of moisture lowered the sliding between grains, leading to an increase in the friction between them. This friction creates a minor resistance to deformation or mobility between the grains, resulting in a higher UCS [10]. However, the elastic modulus decreased dramatically (41%) in this phase (Figure 7). This was due to the dissimilar thermal expansion coefficients of the granodiorite mineral grains, creating new microcracks in the specimens and forcing the microcracks to close under the applied uniaxial compression [71]. As a result, the cracks' closure, new cracks' formation, and irreversible microcrack growth, which were responsible for the difference in the microstructure, produced a low elastic modulus. Furthermore, the crystal and structural water of the minerals would evaporate, resulting in expansion of the grains because of heat treatment. Hence, the dominant factors in this phase were crystal and structural water evaporation, crack closure, new crack creation, and compressive deformation.

Granodiorite is composed of several minerals, each having a unique coefficient of thermal expansion and thermo-elastic features. Hence, due to the asymmetric thermal expansion of the mineral grains' boundaries, the internal stresses were encouraged to build in or between them. Moreover, dehydration, thermal decomposition, and thermal expansion of the rocks and minerals occur at high temperatures. That leads to an increase in cracks and pores, a reduction in density, and mineral alteration [63]. Accordingly, when the temperature of the granodiorite samples was above 400 °C, the mechanical strength and elastic modulus noticeably reduced. Thermal stress and the formation of new inter- and transgranular microcracks generated by high-temperature treatments were attributed to the significant decrease in the UCS (Figure 10b,c). Hence, at a temperature higher than 400 °C, the critical temperature of granodiorite, the mechanical characteristics deteriorated remarkably. Biotite's ability to react with oxygen and change the microstructure of granodiorite may be the reason for this [72]. That aside, variations in the average compressive strength and average elastic modulus of granodiorite rose significantly, which was connected to the α -to- β transition of the quartz [12]. Correspondingly, this stage reflects the onset of phase-change behaviors and mineral alterations in the lattice crystals through the transformation from brittle to plastic. Thus, the failure mode shifted from axial splitting to shear failure (Figure 9).

Furthermore, the stress–strain curve of granodiorite became smoother, and the compaction phase stretched as the temperatures rose, as seen in Figure 8, whereas the elastic modulus declined and the brittleness of granodiorite decreased, which was consistent with earlier research. At 800 °C, the effects of high temperatures were more prominent, and inter- and transgranular cracks were created quickly, building a microcrack network. Furthermore, the granodiorite specimens' interior structures were shattered (Figure 10d), resulting in a significant loss of rock strength values and problematic measurements of E (Table 2).

5.3. Thermal Damage Evolution

Damage mechanics has lately been adopted as a novel technique for studying rock thermodynamics in geotechnical engineering [53]. The anisotropic expansion of granodiorite is connected to thermal damage as a thermal stress concentration emerges between mineral grains, causing microcracking. Once subjected to high temperatures, thermal cracks develop inside the rock and are destroyed when the thermal stress exceeds the bonding energy between the mineral grains [41]. The physical and mechanical characteristics of granodiorite following exposure to high temperatures were investigated in this study. The results indicate that the physical and mechanical features of the samples were modified as the temperature rose. Different criteria can predict the thermal damage characteristic of rock for the thermal damage severity. In this investigation, the thermal damage of granodiorite was estimated by the elastic modulus and the P-wave velocity. A thermal damage index $D(T)$ was specified as the ratio of the parameter at the target temperature to the parameter at room temperature, as indicated in Equations (2) and (3):

$$D(T) = 1 - E_T/E_0 \quad (2)$$

$$D(T) = 1 - (V_{PT}/V_{P0})^2 \quad (3)$$

The rock damage after heating and cooling is almost identical to the thermal cracking mechanism [62]. Hence, changes in the rock microstructure following thermal treatment (Figure 10) can be reflected by the rock thermal damage differences. Figure 11 depicts the relations between temperature, $D(V_p)$, and $D(E)$. Both $D(V_p)$ and $D(E)$ of the granodiorite subjected to thermal treatment rose with the ultimate heating temperature and followed a similar trend. As illustrated in Figure 11, because the P-wave velocities were more sensitive to the temperature than the elastic modulus, the $D(V_p)$ of the granodiorite specimens was higher than $D(E)$ [73]. The thermal damage factor for the studied parameters reached its maximum at 600 °C due to substantial heat damage in the granodiorite microstructure

caused by the higher temperature. Hence, after 600 °C, because of the extreme thermal deterioration in the granodiorite specimens, the measurements of V_p and E were impossible at 800 °C.

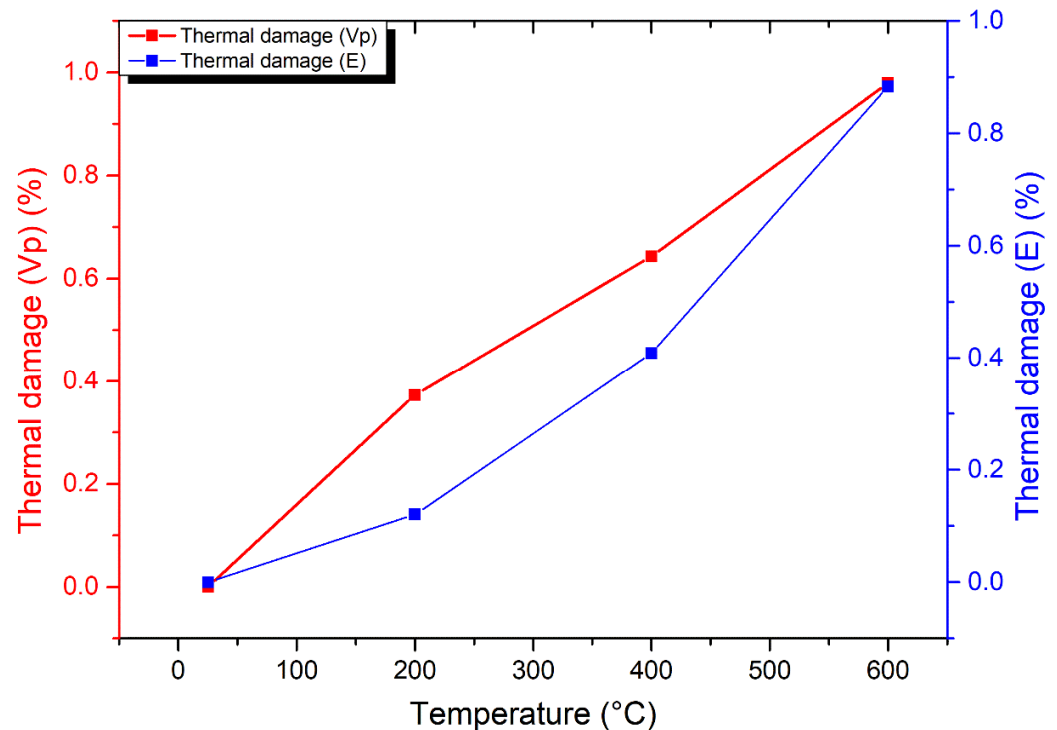


Figure 11. Relations between temperature and thermal damage of granodiorite, described through V_p and E.

5.4. In Comparison to Earlier Investigations

In this part, we assessed the mechanical response of granodiorite to that of other formerly examined granites. However, due to the wide variety of rocks and their compositions, origins, and so on, this research used the normalized value, reflecting the relationships between the UCS and E at the target temperature and those at room temperature (UCS_T/UCS_0 and E_T/E_0). Hence, it was possible to compare the thermal damage's effects on the granodiorite characteristics with other granites. The relationships between the temperatures and the normalized uniaxial compressive strength were obtained, as shown in Figure 12. Aside from that, the relations between the temperatures and normalized elastic modulus are presented in Figure 13.

Based on these findings, it is possible to deduce that the UCS_T/UCS_0 and E_T/E_0 trends with the thermal treatments of granites and granodiorite may rise, fall, or stay constant (Figures 12 and 13) under 400 °C. However, these values “fell only” after this temperature, indicating that 400 °C was the mutation temperature for the rocks investigated. The mechanical features of granodiorite are substantially equivalent to granite when subjected to temperatures up to 400 °C. The characteristics of granodiorite, however, were drastically damaged after this temperature. Consequently, at the mutation range “between 400 and 600 °C”, there was a considerable decrease in the normalized UCS from 1.12% to 0.32% and the normalized E from 0.59% to 0.12% (Figures 12 and 13). Accordingly, due to the ignored value of the UCS at 800 °C, measurements for the elastic modulus were difficult to perform (Table 2).

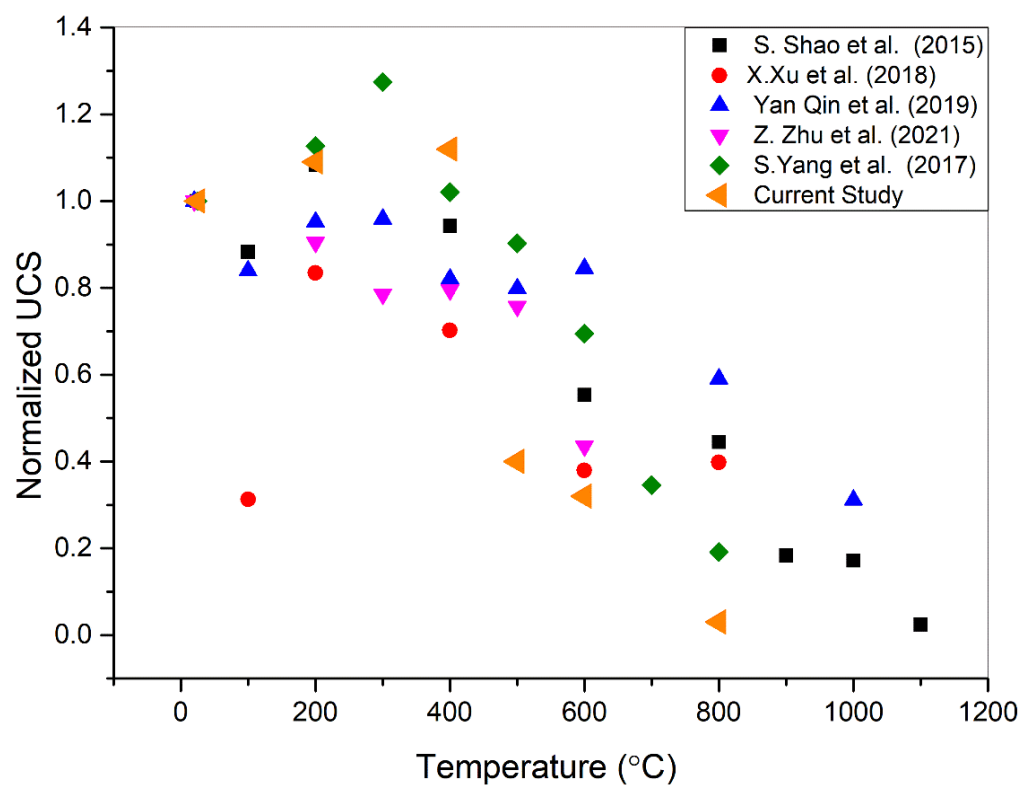


Figure 12. A comparison of the normalized value of UCS of granodiorite with some previous studies on granite heat-treated rock.

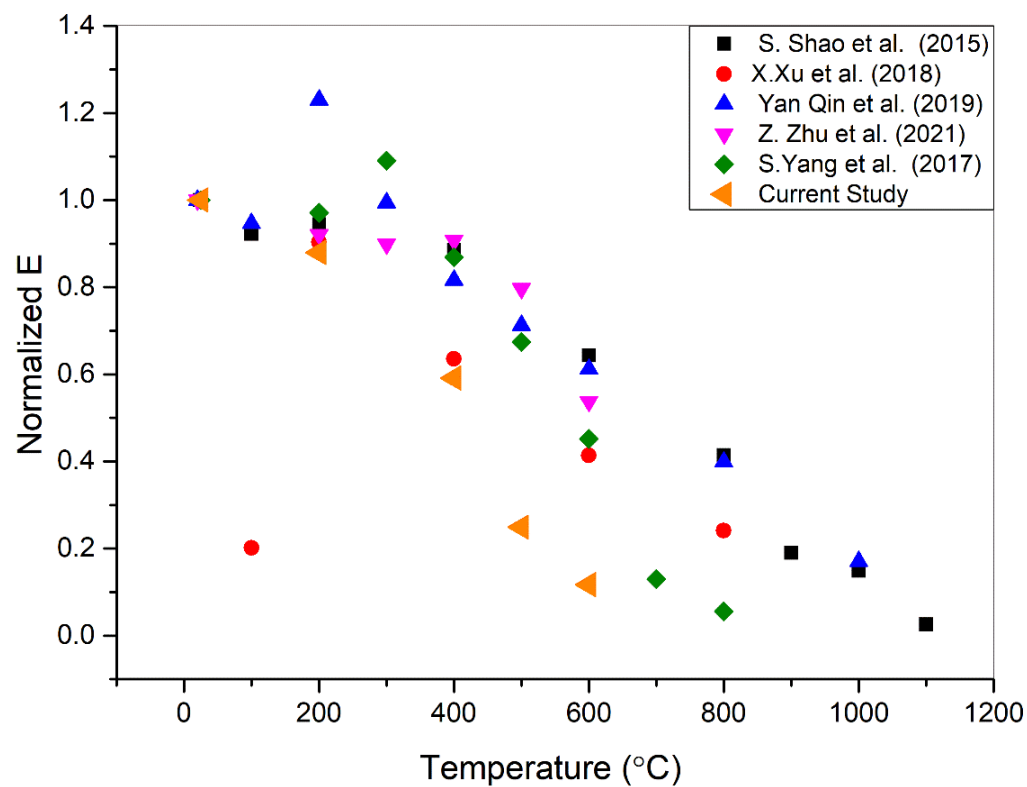


Figure 13. A comparison of the normalized value of E of granodiorite with some early studies on granite heat-treated rock.

One limitation of this work is that sensitivity analysis for model calibration must demonstrate the impact on the results and identify the most important factors [74]. In contrast, the findings of this study provide insights into the physical and mechanical responses and thermal damage of pre-heated granodiorite, which has rarely been investigated, although it is widespread in modern constructions.

6. Conclusions

In this study, thermal treatments of Egyptian granodiorite samples were conducted at temperatures of 200, 400, 500, 600, and 800 °C followed by air cooling to examine its thermo-physical and mechanical responses. A scanning electron microscope was also employed to correlate alterations in the microstructural qualities to changes in the physical and mechanical properties. The following are the main observations:

(1) The density of the Egyptian granodiorite fell after high-temperature exposure because of a loss in mass and a rise in volume, with the latter being the more governing factor up to 600 °C. After 600 °C, the mass loss and volume growth rates both rose considerably, resulting in massive density losses. Furthermore, the average P-wave velocity of the granodiorite dropped approximately linearly with the temperature from 5606 m/s at ambient temperature to 826 m/s at 600 °C.

(2) The UCS of the granodiorite specimens rose at first for the samples heat-treated up to 400 °C due to thermal hardening but then fell linearly between 400 °C and 800 °C. On the other hand, the Young's modulus had a declining trend when the heat treatment temperature rose. Furthermore, due to the interactions and coalescences of the boundary and transgranular cracks, the UCS dropped extensively at 800 °C, explaining the impossible measurement of E.

(3) The temperature affected the failure modes of granodiorite, and two main failure modes may be summarized: the axial splitting mode, which happened at temperatures below 400 °C, and the shear mode, which occurred at temperatures over 400 °C. Furthermore, the granodiorite sample failed more severely, the brittle-ductile transition phase occurred, and the fracture surface became rougher after 400 °C.

(4) When subjected to high temperatures up to 400 °C, the thermal damage for the physical and mechanical responses of granodiorite were nearly identical to granite, according to an exhaustive analysis of granite behavior in some of the former literature and a comparison with granodiorite. However, after this temperature range, the properties of granodiorite were severely degraded.

(5) The temperature threshold of Egyptian granodiorite is 400 °C. This was connected to a substantial drop in density and a P-wave velocity as well as the evolution of the trans-granular cracks detected via SEM, which led to a significant loss in the UCS and E. Consequently, the physical and mechanical responses transitioned from a stable to an unstable state in the mutation range (between 400 and 600 °C). As a result, this temperature must be considered when using granodiorite in thermal applications.

7. Recommendation

Future research may incorporate the sensitivity analysis technique to demonstrate uncertainties in variable inputs like the density, P-wave velocity, UCS, and so on, and their impact on the expected output to identify the most influential factors. Hence, this technique can be involved in the high-complexity modeling process and then overcome.

Author Contributions: Conceptualization, M.E.G.; methodology, M.E.G.; validation, M.E.G. and G.L.; analysis, M.E.G.; writing—original draft, M.E.G.; writing—review and editing, M.E.G., G.L., C.S., J.X., S.Y. and J.L.; supervision, M.E.G. and G.L.; funding acquisition, G.L. All authors have read and agreed to the published version of the manuscript.

Funding: This research was funded by Fundamental Research Funds for the Central Universities (2020ZDYP0221), Project "52174089", supported by the National Natural Science Foundation of China.

Data Availability Statement: Not applicable.

Acknowledgments: The first author greatly appreciates Mohamed Elkarmoty and Mohamed Ismael for their support in carrying out the experiments at the Rock Engineering Laboratory (REL), Faculty of Engineering, Cairo University (FECU), Egypt.

Conflicts of Interest: The authors declare no conflict of interest.

References

- Allison, R.J.; Bristow, G.E. The effects of fire on rock weathering: Some further considerations of laboratory experimental simulation. *Earth Surf. Process. Landf. J. Br. Geomorphol. Res. Gr.* **1999**, *24*, 707–713. [\[CrossRef\]](#)
- Zhu, C.; Arson, C. A thermo-mechanical damage model for rock stiffness during anisotropic crack opening and closure. *Acta Geotech.* **2014**, *9*, 847–867. [\[CrossRef\]](#)
- Zhao, Y.S.; Wan, Z.J.; Feng, Z.J.; Xu, Z.H.; Liang, W.G. Evolution of mechanical properties of granite at high temperature and high pressure. *Geomech. Geophys. Geo-Energy Geo-Resour.* **2017**, *3*, 199–210. [\[CrossRef\]](#)
- Shao, S.; Ranjith, P.G.; Wasantha, P.L.P.; Chen, B.K. Experimental and numerical studies on the mechanical behaviour of Australian Strathbogie granite at high temperatures: An application to geothermal energy. *Geothermics* **2015**, *54*, 96–108. [\[CrossRef\]](#)
- Kumari, W.G.P.; Ranjith, P.G.; Perera, M.S.A.; Chen, B.K.; Abdulagatov, I.M. Temperature-dependent mechanical behaviour of Australian Strathbogie granite with different cooling treatments. *Eng. Geol.* **2017**, *229*, 31–44. [\[CrossRef\]](#)
- Ding, Q.L.; Ju, F.; Mao, X.B.; Ma, D.; Yu, B.Y.; Song, S.B. Experimental Investigation of the Mechanical Behavior in Unloading Conditions of Sandstone after High-Temperature Treatment. *Rock Mech. Rock Eng.* **2016**, *49*, 2641–2653. [\[CrossRef\]](#)
- Burton, E.A.; Upadhye, R.; Friedmann, S.J. *Best Practices in Underground Coal Gasification*; Lawrence Livermore National Lab. (LLNL): Livermore, CA, USA, 2017.
- Verma, A.K.; Gautam, P.; Singh, T.N.; Bajpai, R.K. Discrete element modelling of conceptual deep geological repository for high-level nuclear waste disposal. *Arab. J. Geosci.* **2015**, *8*, 8027–8038. [\[CrossRef\]](#)
- Kourkoulis, S.K. *Fracture and Failure of Natural Building Stones: Applications in the Restoration of Ancient Monuments*; Springer Science & Business Media: Berlin/Heidelberg, Germany, 2007; ISBN 1402050771.
- Zhang, L.; Mao, X.; Lu, A. Experimental study on the mechanical properties of rocks at high temperature. *Sci. China Ser. E Technol. Sci.* **2009**, *52*, 641–646. [\[CrossRef\]](#)
- Jansen, D.P.; Carlson, S.R.; Young, R.P.; Hutchins, D.A. Ultrasonic imaging and acoustic emission monitoring of thermally induced microcracks in Lac du Bonnet granite. *J. Geophys. Res. Solid Earth* **1993**, *98*, 22231–22243. [\[CrossRef\]](#)
- Somerton, W.H. *Thermal Properties and Temperature-Related Behavior of Rock/Fluid Systems*; Elsevier: Amsterdam, The Netherlands, 1992; ISBN 0444890017.
- Li, Q.; Yin, T.; Li, X.; Shu, R. Experimental and Numerical Investigation on Thermal Damage of Granite Subjected to Heating and Cooling. *Mathematics* **2021**, *9*, 3027. [\[CrossRef\]](#)
- Vazquez, P.; Benavente, D.; Montiel, D.; Gomez-Heras, M. Mineralogical Transformations in Granitoids during Heating at Fire-Related Temperatures. *Appl. Sci.* **2021**, *12*, 188. [\[CrossRef\]](#)
- Saksala, T. 3D Numerical Prediction of Thermal Weakening of Granite under Tension. *Geosciences* **2021**, *12*, 10. [\[CrossRef\]](#)
- Tripathi, A.; Gupta, N.; Singh, A.K.; Mohanty, S.P.; Rai, N.; Pain, A. Effects of Elevated Temperatures on the Microstructural, Physico-Mechanical and Elastic Properties of Barakar Sandstone: A Study from One of the World's Largest Underground Coalmine Fire Region, Jharia, India. *Rock Mech. Rock Eng.* **2021**, *54*, 1293–1314. [\[CrossRef\]](#)
- Chakrabarti, B.; Yates, T.; Lewry, A. Effect of fire damage on natural stonework in buildings. *Constr. Build. Mater.* **1996**, *10*, 539–544. [\[CrossRef\]](#)
- Hajpál, M. Changes in sandstones of historical monuments exposed to fire or high temperature. *Fire Technol.* **2002**, *38*, 373–382. [\[CrossRef\]](#)
- Tian, H.; Kempka, T.; Yu, S.; Ziegler, M. Mechanical properties of sandstones exposed to high temperature. *Rock Mech. Rock Eng.* **2016**, *49*, 321–327. [\[CrossRef\]](#)
- Vazquez, P.; Acuña, M.; Benavente, D.; Gibeaux, S.; Navarro, I.; Gomez-Heras, M. Evolution of surface properties of ornamental granitoids exposed to high temperatures. *Constr. Build. Mater.* **2016**, *104*, 263–275. [\[CrossRef\]](#)
- Wong, T.-F. Effects of temperature and pressure on failure and post-failure behavior of Westerly granite. *Mech. Mater.* **1982**, *1*, 3–17. [\[CrossRef\]](#)
- Chaki, S.; Takarli, M.; Agbodjan, W.P. Influence of thermal damage on physical properties of a granite rock: Porosity, permeability and ultrasonic wave evolutions. *Constr. Build. Mater.* **2008**, *22*, 1456–1461. [\[CrossRef\]](#)
- Liu, S.; Xu, J. Mechanical properties of Qinling biotite granite after high temperature treatment. *Int. J. Rock Mech. Min. Sci.* **2014**, *71*, 188–193. [\[CrossRef\]](#)
- Yang, S.-Q.; Ranjith, P.G.; Jing, H.-W.; Tian, W.-L.; Ju, Y. An experimental investigation on thermal damage and failure mechanical behavior of granite after exposure to different high temperature treatments. *Geothermics* **2017**, *65*, 180–197. [\[CrossRef\]](#)
- Chandrasekharam, D.; Pabasara Kumari, W.G.; Avanthi Isaka, B.L.; Gamage, R.P.; Rathnaweera, T.D.; Anne Perera, M.S. An influence of thermally-induced micro-cracking under cooling treatments: Mechanical characteristics of Australian granite. *Energies* **2018**, *11*, 1338. [\[CrossRef\]](#)

26. Kant, M.A.; Ammann, J.; Rossi, E.; Madonna, C.; Höser, D.; Rudolf von Rohr, P. Thermal properties of Central Aare granite for temperatures up to 500 °C: Irreversible changes due to thermal crack formation. *Geophys. Res. Lett.* **2017**, *44*, 771–776. [[CrossRef](#)]
27. Liu, S.; Xu, J. Study on dynamic characteristics of marble under impact loading and high temperature. *Int. J. Rock Mech. Min. Sci.* **2013**, *62*, 51–58. [[CrossRef](#)]
28. Peng, J.; Rong, G.; Cai, M.; Yao, M.-D.; Zhou, C.-B. Physical and mechanical behaviors of a thermal-damaged coarse marble under uniaxial compression. *Eng. Geol.* **2016**, *200*, 88–93. [[CrossRef](#)]
29. Vagnon, F.; Colombero, C.; Colombo, F.; Comina, C.; Ferrero, A.M.; Mandrone, G.; Vinciguerra, S.C. Effects of thermal treatment on physical and mechanical properties of Valdieri Marble—NW Italy. *Int. J. Rock Mech. Min. Sci.* **2019**, *116*, 75–86. [[CrossRef](#)]
30. Sirdesai, N.N.; Mahanta, B.; Ranjith, P.G.; Singh, T.N. Effects of thermal treatment on physico-morphological properties of Indian fine-grained sandstone. *Bull. Eng. Geol. Environ.* **2019**, *78*, 883–897. [[CrossRef](#)]
31. Zhang, W.; Sun, Q.; Zhu, Y.; Guo, W. Experimental study on response characteristics of micro–macroscopic performance of red sandstone after high-temperature treatment. *J. Therm. Anal. Calorim.* **2019**, *136*, 1935–1945. [[CrossRef](#)]
32. Mohamadi, M.; Wan, R.G. Strength and post-peak response of Colorado shale at high pressure and temperature. *Int. J. Rock Mech. Min. Sci.* **2016**, *84*, 34–46. [[CrossRef](#)]
33. Liang, W.G.; Xu, S.G.; Zhao, Y.S. Experimental study of temperature effects on physical and mechanical characteristics of salt rock. *Rock Mech. Rock Eng.* **2006**, *39*, 469–482. [[CrossRef](#)]
34. Killc, Ö. The influence of high temperatures on limestone P-wave velocity and Schmidt hammer strength. *Int. J. Rock Mech. Min. Sci.* **2006**, *43*, 980–986. [[CrossRef](#)]
35. Zhang, W.; Sun, Q.; Zhu, S.; Wang, B. Experimental study on mechanical and porous characteristics of limestone affected by high temperature. *Appl. Therm. Eng.* **2017**, *110*, 356–362. [[CrossRef](#)]
36. Luo, J.; Wang, L. High-temperature mechanical properties of mudstone in the process of underground coal gasification. *Rock Mech. Rock Eng.* **2011**, *44*, 749–754. [[CrossRef](#)]
37. Zhang, L.; Mao, X.; Liu, R.; Li, Y.; Yin, H. Meso-structure and fracture mechanism of mudstone at high temperature. *Int. J. Min. Sci. Technol.* **2014**, *24*, 433–439. [[CrossRef](#)]
38. Liu, X.; Zhang, C.; Yuan, S.; Fityus, S.; Sloan, S.W.; Buzzi, O. Effect of High Temperature on Mineralogy, Microstructure, Shear Stiffness and Tensile Strength of Two Australian Mudstones. *Rock Mech. Rock Eng.* **2016**, *49*, 3513–3524. [[CrossRef](#)]
39. Huang, Y.-H.; Yang, S.-Q.; Tian, W.-L.; Zhao, J.; Ma, D.; Zhang, C.-S. Physical and mechanical behavior of granite containing pre-existing holes after high temperature treatment. *Arch. Civ. Mech. Eng.* **2017**, *17*, 912–925. [[CrossRef](#)]
40. Ohno, I.; Harada, K.; Yoshitomi, C. Temperature variation of elastic constants of quartz across the α - β transition. *Phys. Chem. Miner.* **2006**, *33*, 1–9. [[CrossRef](#)]
41. Sippel, J.; Siegesmund, S.; Weiss, T.; Nitsch, K.-H.; Korzen, M. Decay of natural stones caused by fire damage. *Geol. Soc. Lond. Spec. Publ.* **2007**, *271*, 139–151. [[CrossRef](#)]
42. Keshavarz, M.; Pellet, F.L.; Loret, B. Damage and changes in mechanical properties of a gabbro thermally loaded up to 1000 °C. *Pure Appl. Geophys.* **2010**, *167*, 1511–1523. [[CrossRef](#)]
43. Inserra, C.; Biwa, S.; Chen, Y. Influence of thermal damage on linear and nonlinear acoustic properties of granite. *Int. J. Rock Mech. Min. Sci.* **2013**, *62*, 96–104. [[CrossRef](#)]
44. Sha, S.; Rong, G.; Peng, J.; Li, B.; Wu, Z. Effect of open-fire-induced damage on Brazilian tensile strength and microstructure of granite. *Rock Mech. Rock Eng.* **2019**, *52*, 4189–4202. [[CrossRef](#)]
45. Abbaszadeh Shahri, A.; Ashoghi, R.; Khorsand Zak, M. A hybridized intelligence model to improve the predictability level of strength index parameters of rocks. *Neural Comput. Appl.* **2021**, *33*, 3841–3854. [[CrossRef](#)]
46. Teymen, A. Statistical models for estimating the uniaxial compressive strength and elastic modulus of rocks from different hardness test methods. *Heliyon* **2021**, *7*, e06891. [[CrossRef](#)] [[PubMed](#)]
47. Zhang, Y.; Zhang, X.; Zhao, Y. Process of sandstone thermal cracking. *Chin. J. Geophys.* **2005**, *48*, 722–726. [[CrossRef](#)]
48. Freire-Lista, D.M.; Fort, R.; Varas-Muriel, M. Thermal stress-induced microcracking in building granite. *Eng. Geol.* **2016**, *206*, 83–93. [[CrossRef](#)]
49. Zhu, Z.; Tian, H.; Mei, G.; Jiang, G.; Dou, B.; Xiao, P. Experimental investigation on mechanical behaviors of Nanang granite after thermal treatment under conventional triaxial compression. *Environ. Earth Sci.* **2021**, *80*, 46. [[CrossRef](#)]
50. Ferrero, A.M.; Marini, P. Experimental studies on the mechanical behaviour of two thermal cracked marbles. *Rock Mech. Rock Eng.* **2001**, *34*, 57–66. [[CrossRef](#)]
51. Wu, X.; Huang, Z.; Zhang, S.; Cheng, Z.; Li, R.; Song, H.; Wen, H.; Huang, P. Damage Analysis of High-Temperature Rocks Subjected to LN₂ Thermal Shock. *Rock Mech. Rock Eng.* **2019**, *52*, 2585–2603. [[CrossRef](#)]
52. Zhao, Y.; Wan, Z.; Feng, Z.; Yang, D.; Zhang, Y.; Qu, F. Triaxial compression system for rock testing under high temperature and high pressure. *Int. J. Rock Mech. Min. Sci.* **2012**, *52*, 132–138. [[CrossRef](#)]
53. Liu, S.; Xu, J. An experimental study on the physico-mechanical properties of two post-high-temperature rocks. *Eng. Geol.* **2015**, *185*, 63–70. [[CrossRef](#)]
54. Tian, H.; Ziegler, M.; Kempka, T. Physical and mechanical behavior of claystone exposed to temperatures up to 1000 °C. *Int. J. Rock Mech. Min. Sci.* **2014**, *70*, 144–153. [[CrossRef](#)]

55. Kumari, W.G.P.; Beaumont, D.M.; Ranjith, P.G.; Perera, M.S.A.; Avanthi Isaka, B.L.; Khandelwal, M. An experimental study on tensile characteristics of granite rocks exposed to different high-temperature treatments. *Geomech. Geophys. Geo-Energy Geo-Resour.* **2019**, *5*, 47–64. [[CrossRef](#)]
56. Chen, Y.L.; Ni, J.; Shao, W.; Azzam, R. Experimental study on the influence of temperature on the mechanical properties of granite under uni-axial compression and fatigue loading. *Int. J. Rock Mech. Min. Sci.* **2012**, *56*, 62–66. [[CrossRef](#)]
57. El-Taher, A.; Uosif, M.A.M.; Orabi, A.A. Natural radioactivity levels and radiation hazard indices in granite from Aswan to Wadi El-Allaqa southeastern desert, Egypt. *Radiat. Prot. Dosim.* **2007**, *124*, 148–154. [[CrossRef](#)] [[PubMed](#)]
58. Rock, A.C.D. *Standard Test Method for Compressive Strength and Elastic Moduli of Intact Rock Core Specimens under Varying States of Stress and Temperatures*; ASTM International: West Conshohocken, PA, USA, 2010.
59. Kim, K.M.; Kemeny, J. Effect of thermal shock and rapid unloading on mechanical rock properties. In Proceedings of the 43rd US Rock Mechanics Symposium & 4th US, Canada Rock Mechanics Symposium, Asheville, NC, USA, 28 June–1 July 2009.
60. Gomah, M.E.; Li, G.; Bader, S.; Elkarmoty, M.; Ismael, M. Damage Evolution of Granodiorite after Heating and Cooling Treatments. *Minerals* **2021**, *11*, 779. [[CrossRef](#)]
61. Zhang, W.; Sun, Q.; Hao, S.; Geng, J.; Lv, C. Experimental study on the variation of physical and mechanical properties of rock after high temperature treatment. *Appl. Therm. Eng.* **2016**, *98*, 1297–1304. [[CrossRef](#)]
62. Zhang, J.; Shen, Y.; Yang, G.; Zhang, H.; Wang, Y.; Hou, X.; Sun, Q.; Li, G. Inconsistency of changes in uniaxial compressive strength and P-wave velocity of sandstone after temperature treatments. *J. Rock Mech. Geotech. Eng.* **2021**, *13*, 143–153. [[CrossRef](#)]
63. Gautam, P.K.; Verma, A.K.; Jha, M.K.; Sharma, P.; Singh, T.N. Effect of high temperature on physical and mechanical properties of Jalore granite. *J. Appl. Geophys.* **2018**, *159*, 460–474. [[CrossRef](#)]
64. Cai, C.; Li, G.; Huang, Z.; Tian, S.; Shen, Z.; Fu, X. Experiment of coal damage due to super-cooling with liquid nitrogen. *J. Nat. Gas Sci. Eng.* **2015**, *22*, 42–48. [[CrossRef](#)]
65. Homand-Etienne, F.; Houpert, R. Thermally induced microcracking in granites: Characterization and analysis. In *International Journal of Rock Mechanics and Mining Sciences & Geomechanics Abstracts*; Elsevier: Amsterdam, The Netherlands, 1989; Volume 26, pp. 125–134.
66. Abbaszadeh Shahri, A.; Larsson, S.; Johansson, F. Updated relations for the uniaxial compressive strength of marlstones based on P-wave velocity and point load index test. *Innov. Infrastruct. Solut.* **2016**, *1*, 17. [[CrossRef](#)]
67. Hale, P.A.; Shakoor, A. A laboratory investigation of the effects of cyclic heating and cooling, wetting and drying, and freezing and thawing on the compressive strength of selected sandstones. *Environ. Eng. Geosci.* **2003**, *9*, 117–130. [[CrossRef](#)]
68. Vázquez, P.; Shushakova, V.; Gómez-Heras, M. Influence of mineralogy on granite decay induced by temperature increase: Experimental observations and stress simulation. *Eng. Geol.* **2015**, *189*, 58–67. [[CrossRef](#)]
69. Zhang, B.; Tian, H.; Dou, B.; Zheng, J.; Chen, J.; Zhu, Z.; Liu, H. Macroscopic and microscopic experimental research on granite properties after high-temperature and water-cooling cycles. *Geothermics* **2021**, *93*, 102079. [[CrossRef](#)]
70. Hajpál, M.; Török, Á. Mineralogical and colour changes of quartz sandstones by heat. *Environ. Geol.* **2004**, *46*, 311–322. [[CrossRef](#)]
71. Singh, B.; Ranjith, P.G.; Chandrasekharam, D.; Viete, D.; Singh, H.K.; Lashin, A.; Al Arifi, N. Thermo-mechanical properties of Bundelkhand granite near Jhansi, India. *Geomech. Geophys. Geo-Energy Geo-Resour.* **2015**, *1*, 35–53. [[CrossRef](#)]
72. Pavese, A.; Curetti, N.; Diella, V.; Levy, D.; Dapiaggi, M.; Russo, U. P-V and T-V Equations of State of natural biotite: An in-situ high-pressure and high-temperature powder diffraction study, combined with Mössbauer spectroscopy. *Am. Mineral.* **2007**, *92*, 1158–1164. [[CrossRef](#)]
73. Zhu, Z.; Kempka, T.; Ranjith, P.G.; Tian, H.; Jiang, G.; Dou, B.; Mei, G. Changes in thermomechanical properties due to air and water cooling of hot dry granite rocks under unconfined compression. *Renew. Energy* **2021**, *170*, 562–573. [[CrossRef](#)]
74. Asheghi, R.; Hosseini, S.A.; Saneie, M.; Shahri, A.A. Updating the neural network sediment load models using different sensitivity analysis methods: A regional application. *J. Hydroinform.* **2020**, *22*, 562–577. [[CrossRef](#)]